$K_2Na(I_3O_8)_3$: a promising mid-infrared birefringent material with two different structures of octaoxotriiodate(V) polyanions

Min-Quan Lin,[a,b,e] Meng-Fan Duan,[b,c,e] Jiang-Gao Mao[b,d,e] and Bing-Ping Yang*[b,d,e]

a. College of Chemistry, Fuzhou University, Fuzhou, 350108, P.R. China.

b. State Key Laboratory of Structural Chemistry, Fujian Institute of Research on the Structure of Matter, Chinese Academy of Sciences, Fuzhou, 350002, P.R. China.

c. College of Chemistry and Materials Science, Fujian Normal University, Fuzhou, 350007, P.R. China

d. University of Chinese Academy of Sciences, Beijing, 100039, P.R. China.

e. Fujian College, University of Chinese Academy of Sciences, Fuzhou 350002, P.R. China

Table of contents

Section	Title	Page
S1	Experimental Methods	S3
S2	Computational Methods	S3
Table S1	Space groups, polyiodate units and birefringence of some polyiodates.	S5
Table S2	Crystallographic data and structure refinement parameters of $K_2Na(I_3O_8)_3$.	S6
Table S3	Fractional atomic coordinates ($\times10^4$), equivalent isotropic displacement parameters ($Å^2\times10^3$) and bond valence sums (BVS) of $K_2Na(I_3O_8)_3$. U_{eq} is defined as 1/3 of the trace of the orthogonalised U_{ij} tensor.	S7
Table S4	Selected bond lengths of $K_2Na(I_3O_8)_3$.	S8
Table S5	Selected bond angles of $K_2Na(I_3O_8)_3$.	S8
Table S6	Angle of the lone electron pairs in each unit with respect to the coordinate axis.	S9
Figure S1	Simulated and measured PXRD patterns of $K_2Na(I_3O_8)_3$.	S10
Figure S2	TGA and DTA curves of $K_2Na(I_3O_8)_3$ under a N_2 atmosphere.	S10
Figure S3	Arrangement of octaoxotriiodate(V) polyanions in the structure of $K_2Na(I_3O_8)_3$.	S11
Reference		S12

S1 Experimental Methods

Reagents and Instruments. The starting materials, $NaIO_3$, KOH, I_2O_5, and H_3PO_4, were purchased from commercial sources and used without further purification.

Single crystal structure determination. The $K_2Na(I_3O_8)_3$ crystals were cut to the requisite dimensions and a high quality crystal was selected, mounted on a glass fiber, and inserted into the goniometer head for single crystal structural determination. Diffraction data were collected on a Rigaku Oxford Diffraction SuperNova CCD diffractometer using Mo Kα radiation (λ = 0.71073 Å) at 294.86 K. Cell refinement and data reduction were performed using CrysAlisPro. Numerical absorption correction based on Gaussian integration over a multifaceted crystal model and empirical absorption correction using spherical harmonics were implemented in the SCALE3 ABSPACK scaling algorithm.[1] The structure was determined by the direct method and refined by full-matrix least-squares fitting on F^2 using SHELXL.[2,3] All of the atoms were refined with anisotropic thermal parameters. The structure was checked for missing symmetry elements using PLATON, and none was suggested.[4] The Flack parameter was refined to 0.01(5) for the title compound, indicating the correctness of the absolute structure.[5] Crystallographic data and structural refinements of the compound are given in Table S1, and some selected bond lengths and angles are given in Tables S3 and S4.

Powder X-ray Diffraction (PXRD). PXRD analysis was performed on a Rigaku MiniFlex600 diffractometer equipped with a graphite monochromator using Cu Kα radiation (λ = 1.54186 Å) in the 2θ range of 10–60° with a scan step width of 0.02°.

Spectroscopic Measurements. IR spectra were recorded on a Bruker Vertex 70 spectrometer with air as background in the range of 4000–400 cm^{-1} with a resolution of 2 cm^{-1} at room temperature. The UV-vis-NIR diffuse reflectance spectrum in the 200–2000 nm range was recorded on a PerkinElmer Lambda 950 UV-vis-NIR spectrophotometer using a $BaSO_4$ powder plate used as a 100% reflectance reference. Absorption data were calculated from the diffuse reflectance data using the Kubelka-Munk function: $\alpha/S = (1-R)^2/2R$, where α is the absorption coefficient and S is the scattering coefficient.[6] Extrapolation of the absorption edge to the baseline in the α/S versus Energy plot gives the band gap value.

Thermal Analyses. Thermogravimetric analysis (TGA) and differential thermal analysis (DTA) were performed on a NETZCH STA 499C installation. Powder samples of approximately 3.0–5.0 mg were placed in an alumina crucible and heated from 20 to 1000 °C at a rate of 15 °C min^{-1} under a nitrogen atmosphere.

Birefringence Measurements. The birefringence of $K_2Na(I_3O_8)_3$ was measured with a polarizing light microscope (ZEISS Axio Scope A1), by means of tilting the compensator and compensating the optical path difference. The birefringence was calculated according to Eqn. (1):

$$R = \Delta n \times T$$

where R denotes the optical path difference, Δn represents the birefringence, and T is the thickness of the crystal.

S2. Computational Methods

The calculations of the electronic and optical properties were performed with the CASTEP code using the plane-wave pseudopotential density functional theory (DFT).[7,8] The generalized gradient approximation (GGA) Perdew-Burke-Ernzerhof (PBE) was chosen as the exchange correlation functional.[9] The core electron interactions were represented by the norm-conserving pseudopotential.[10] Na $3s^1$, K $4s^1$, I $5s^25p^5$, O $2s^22p^4$ orbital electrons were set as the valence electrons. A cutoff energy of 750 eV was used to determine of the number of plane-wave basis sets. The Monkhorst-Pack k-point sampling was 2 × 2 × 2 for numerical integration over the Brillouin zone. More than 240 empty bands were used in the optical property calculations.

The calculations of the second-order NLO susceptibilities were based on the length gauge formalism within the independent particle approximation.[11,12] The second-order NLO susceptibility can be expressed as $\chi_{L}^{abc}(-2\omega;\ \omega,\ \omega)=\chi_{inter}^{abc}(-2\omega;\ \omega,\ \omega)+\chi_{intra}^{abc}(-2\omega;\ \omega,\ \omega)+\chi_{mod}^{abc}(-2\omega;\ \omega,\ \omega)$, where the subscript L denotes the length gauge, χ_{inter}^{abc}, χ_{intra}^{abc} and χ_{mod}^{abc} give the contributions to χ_{L}^{abc} from interband processes, intraband processes, and the modulation of interband terms by intraband terms, respectively.

To gain further understanding of the anion groups, the electronic structures of the IO_3^- and $[I_3O_8]^-$ groups at the molecular level were calculated by the DFT method implemented by the Gaussian09 package at the B3LYP/LANL2DZ level.

Table S1. Space groups, polyiodate units and birefringence of some polyiodates.

Compounds	Space Group	Birefringence	Reference
GdI_5O_{14}	*Cm*	Δn_{cal} = 0.092 @ 1064 nm	13
YI_5O_{14}	*Cm*	Δn_{cal} = 0.091 @ 1064 nm	13
$Ba_4Ag_5(IO_3)_6(I_3O_8)_3(I_4O_{11})_2$	*Pnc*2	Δn_{cal} = 0.082 @ 1064 nm	14
NaI_3O_8	*P*-4	Δn_{cal} = 0.225 @ 1064 nm	15
α-AgI_3O_8	*Pnc*2	Δn_{cal} = 0.208 @ 1064 nm	16
β-AgI_3O_8	*I*-4	Δn_{cal} = 0.210 @ 1064 nm	16
$K_2Na(IO_3)_2(I_3O_8)$	*Pc*	Δn_{cal} = 0.055 @ 1064 nm	17
$C(NH_2)_3Rb(I_3O_8)(IO_3)(I_2O_6H_2)$	*P*-1	Δn_{cal} = 0.286 @ 1064 nm	18
$C(NH_2)_3(I_3O_8)(HI_3O_8)(H_2I_2O_6)(HIO_3)_4\cdot 3H_2O$	*P*1	Δn_{exp} = 0.059 @ 550 nm	19
$K_2BiI_5O_{15}$	*Abm*2	Δn_{cal} = 0.0536 @ 1064 nm	20
$Rb_2BiI_5O_{15}$	*Abm*2	Δn_{cal} = 0.0427 @ 1064 nm	20
SrI_3O_9H	$P2_1/c$	Δn_{cal} = 0.07 @ 1064 nm	21
$[o\text{-}C_5H_4NHOH]_2[I_7O_{18}(OH)]\cdot 3H_2O$	*Ia*	Δn_{cal} = 0.114 @ 1064 nm	22
$Pb_4O(IO_3)_3(I_3O_7F_3)BF_4$	*R*3*c*	Δn_{exp} = 0.09 @ 546.1 nm	23
$Sr_4O(IO_3)_3(I_3O_7F_3)BF_4$	*R*3*c*	Δn_{exp} = 0.08 @ 546.1 nm	23
$BaI_2O_5F_2$	$P2_1/c$	Δn_{exp} = 0.174 @ 1064 nm	24
$SrI_2O_5F_2$	$P2_1/c$	Δn_{exp} = 0.203 @ 532 nm	25

Table S2. Crystallographic data and structure refinement parameters of $K_2Na(I_3O_8)_3$.

Formula	$K_2Na(I_3O_8)_3$
Formula weight	1627.29
Temperature/K	296.3(5)
Crystal system	orthorhombic
Space group	*Pnna*
a/Å	11.6040(11)
b/Å	24.366(2)
c/Å	8.4503(7)
α/°	90
β/°	90
γ/°	90
V/Å^3	2389.2(4)
Z	4
ρ_{calc}g/cm^3	4.524
μ/mm^{-1}	12.149
F(000)	2872.0
Radiation	MoK*α* (λ = 0.71073)
Independent reflections	3013 [R_{int} = 0.0564, R_{sigma} = 0.0485]
Goodness-of-fit on F^2	1.049
Final R indexes [I>=2σ (I)]	R_1 = 0.0349, wR_2 = 0.0716
Final R indexes [all data]	R_1 = 0.0501, wR_2 = 0.0811
Flack parameter	−0.05(3)

[a] $R_1 = \Sigma||F_o|-|F_c||/\Sigma|F_o|$, $wR_2 = \{\Sigma[w(F_o^2-F_c^2)^2]/\Sigma[w(F_o^2)^2]\}^{1/2}$

Table S3. Fractional atomic coordinates ($\times 10^4$), equivalent isotropic displacement parameters ($Å^2 \times 10^3$) and bond valence sums (BVS) of $K_2Na(I_3O_8)_3$. U_{eq} is defined as 1/3 of the trace of the orthogonalised U_{ij} tensor.

Atom	x	y	z	U(eq)	BVS
I3	4991.4(4)	5681.7(2)	2758.1(5)	13.36(12)	4.936
I4	4490.1(4)	4245.8(2)	2404.2(5)	12.74(12)	5.175
I5	3292.0(4)	3275.2(2)	4688.3(5)	12.96(12)	4.884
I1	9064.8(5)	7500	2500	11.80(15)	5.276
I2	7795.3(4)	6631.4(2)	-86.7(5)	13.01(12)	4.952
K2	7500	5000	345(2)	20.5(5)	1.433
K1	9904(2)	7500	-2500	23.1(5)	1.204
Na1	2500	5000	5118(4)	22.4(10)	1.286
O10	4418(4)	3414.0(19)	3122(5)	17.0(11)	2.092
O2	8961(4)	7168(2)	287(5)	20.1(11)	2.195
O7	4300(5)	5056(2)	1762(6)	25.4(12)	2.121
O12	3580(5)	2559(2)	4652(6)	22.4(12)	1.842
O3	8079(5)	6661(2)	-2162(5)	19.7(11)	1.798
O9	3254(4)	4312(2)	3642(6)	20.0(11)	1.812
O1	8085(5)	8037(2)	1929(6)	22.5(12)	1.736
O6	4386(5)	5586(2)	4670(5)	23.3(12)	1.842
O4	8595(5)	6040(2)	451(6)	23.6(12)	1.862
O8	3835(4)	4076.7(19)	547(5)	15.9(10)	1.973
O5	6382(5)	5378(2)	2895(6)	24.5(12)	1.832
O11	4192(5)	3462(2)	6353(6)	22.9(12)	2.016

Table S4. Selected bond lengths of $K_2Na(I_3O_8)_3$.

Bond	Bond length/Å	Bond	Bond length/Å
I1−O1	1.799(5)	I3−O7	1.917(5)
I1−O1[4]	1.799(5)	I4−O7	2.059(5)
I1−O2	2.041(4)	I4−O8	1.792(4)
I1−O2[1]	2.041(4)	I4−O9	1.783(5)
I2−O2	1.908(5)	I4−O10	2.117(5)
I2−O3	1.786(4)	I5−O10	1.890(5)
I2−O4	1.772(5)	I5−O11	1.811(5)
I3−O5	1.780(5)	I5−O12	1.778(5)
I3−O6	1.777(5)		

Symmetry transformations for the atoms generated: [1]1-X,1-Y,1-Z; [2]1-X,1-Y,-Z; [3]3/2-X,1-Y,1+Z; [4]+X,3/2-Y,1/2-Z; [5]1/2+X,+Y,-Z; [6]3/2-X,1-Y,+Z; [7]3/2-X,1/2+Y,1/2-Z; [8]3/2-X,1-Y,-1+Z; [9]+X,3/2-Y,-1/2-Z; [10]1/2-X,1-Y,+Z; [11]1/2+X,+Y,1-Z.

Table S5. Selected bond angles of $K_2Na(I_3O_8)_3$.

Bond angle	Degree	Bond angle	Degree
O1-I1-O2	90.3(2)	O7-I3-O11[1]	171.52(18)
O1-I1-O2[4]	85.4(2)	O7-I4-O10	171.5(2)
O1[4]-I1-O2	85.4(2)	O8-I4-O7	86.8(2)
O1[4]-I1-O2[4]	90.3(2)	O8-I4-O10	90.8(2)
O1[4]-I1-O1	101.6(4)	O9-I4-O8	101.2(2)
O2-I1-O2[4]	173.2(3)	O9-I4-O7	88.9(2)
O3-I2-O2	90.3(2)	O11-I5-O10	95.8(2)
O4-I2-O2	98.2(2)	O12-I5-O11	98.7(2)
O4-I2-O3	100.8(2)	O12-I5-O10	91.9(2)
O5-I3-O7	94.4(2)	I2-O2-I1	117.7(2)
O5-I3-O11[1]	89.1(2)	I5-O10-I4	113.5(2)
O6-I3-O5	104.2(2)	I3-O7-I4	127.0(2)
O6-I3-O11[1]	89.2(2)	I5-O11-I3[1]	133.3(3)
O6-I3-O7	97.4(2)		

Symmetry transformations for the atoms generated: [1]1-X,1-Y,1-Z; [2]1-X,1-Y,-Z; [3]3/2-X,1-Y,1+Z; [4]+X,3/2-Y,1/2-Z; [5]1/2+X,+Y,-Z; [6]3/2-X,1-Y,+Z; [7]3/2-X,1/2+Y,1/2-Z; [8]3/2-X,1-Y,-1+Z; [9]+X,3/2-Y,-1/2-Z; [10]1/2-X,1-Y,+Z; [11]1/2+X,+Y,1-Z.

Table S6. Angle of the lone electron pairs in each unit with respect to the coordinate axis.

Unit	*a*-axis	*b*-axis	*c*-axis
$I(1)O_4$	0°	90°	90°
$I(2)O_3$	24.84°	82.14°	66.60°
$I(3)O_3$	83.58°	31.62°	64.76°
$I(4)O_4$	12.31°	85.76°	78.50°
$I(5)O_3$	24.15°	66.37°	85.24°

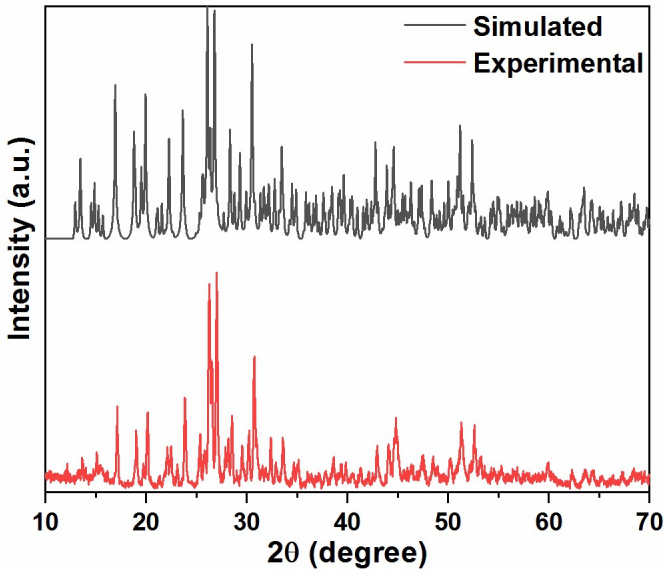

Figure S1. Simulated and measured PXRD patterns of $K_2Na(I_3O_8)_3$.

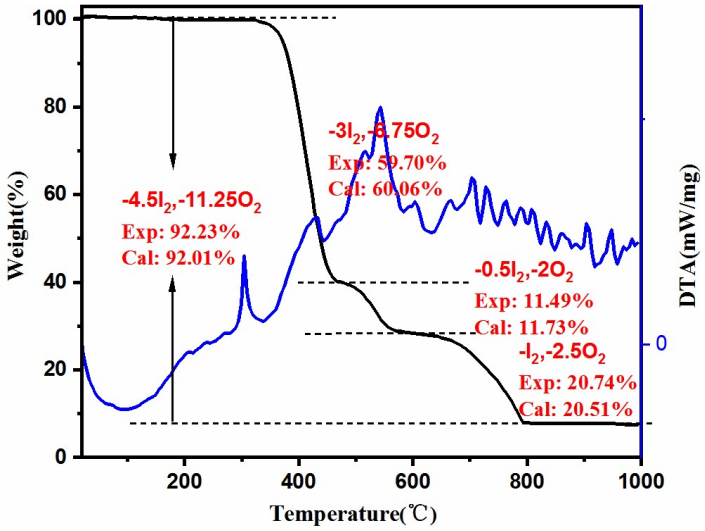

Figure S2. TGA and DTA curves of $K_2Na(I_3O_8)_3$ under a N_2 atmosphere.

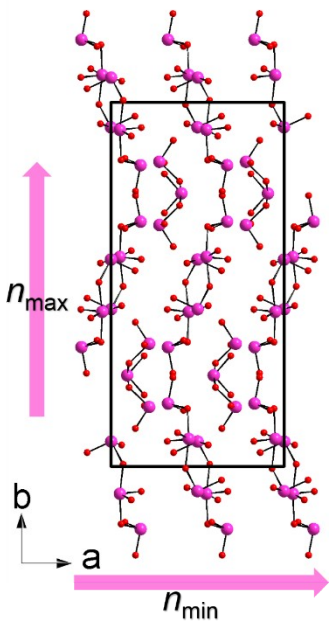

Figure S3. Arrangement of octaoxotriiodate(V) polyanions in the structure of $K_2Na(I_3O_8)_3$.

References

1 Weeks, C. M.; Hauptman, H. A.; Smith, G. D.; Blessing, R. H.; Teeter, M. M.; Miller, R., *Acta Crystallogr., Sect D: Biol. Crystallogr.* 1995, **51 (1)**, 33–38.

2 Sheldrick, G. M., *Sect C: Cryst. Struct. Commun.* 2015, **71 (1)**, 3–8.

3 Sheldrick, G. M., *Acta Crystallogr., Sect C: Cryst. Struct. Commun.* 2015, **71 (1)**, 3–8.

4 Spek, A. L., J. *Appl. Crystallogr.* 2003, **36 (1)**, 7–13.

5 Flack, H. D., *Sect A: Found. Crystallogr.* 1983, **39 (6)**, 876–881.

6 Kubelka; Munk. Zeit. *Für Tekn. Physik,* 1931, **12**, 593.

7 Milman, V.; Winkler, B.; White, J. A.; Pickard, C. J.; Payne, M. C.; Akhmatskaya, E. V.; Nobes, R. H., Int. J. *Quantum Chem.* 2000, **77 (5)**, 895–910.

8 M D Segall; Philip J D Lindan; M J Probert; C J Pickard; P J Hasnip; S J Clark; M C Payne., J. *Phys.: Condens. Matter.* 2002, **14 (11)**, 2717.

9 Perdew, J. P.; Burke, K.; Ernzerhof, M., *Phys. Rev. Lett.* 1996, **77 (18)**, 3865–3868.

10 Lin, J. S.; Qteish, A., *Phys. Rev. B* 1993, **47 (8)**, 4174–4180.

11 Sharma, S.; Dewhurst, J. K., *Phys. Rev. B* 2003, **67 (16)**, 165332.

12 Sipe, J. E.; Ghahramani, E., *Phys. Rev. B* 1993, **48 (16)**, 11705–11722.

13 J. Chen, C.-L. Hu, F.-F. Mao, B.-P. Yang, X.-H. Zhang, J.-G. Mao, *Angew. Chem. Int. Ed.* 2019, **58**, 11666–11669.

14 J. Chen, Q.-Q. Chen, F.-F. Mao, Z. Liu, B.-X. Li, X.-H. Wu, K.-Z. Du, *Inorg. Chem. Front.* 2022, **9**, 5917–5925.

15 D. Phanon, I. Gautier-Luneau, *Angew. Chem. Int. Ed.* 2007, **46**, 8488–8491.

16 X. Xu, C.-L. Hu, B.-X. Li, B.-P. Yang, J.-G. Mao, *Chem. Mater.* 2014, **26**, 3219–3230.

17 T. Abudouwufu, M. Zhang, S. Cheng, H. Zeng, Z. Yang, S. Pan, *Chem. Mater.* 2020, **32**, 3608–3614.

18 D. Yan, Y. Ma, R.-L. Tang, L. Hu, F.-F. Mao, J. Zheng, X.-D. Zhang, S.-F. Li, *J. Solid State Chem.* 2022, **315**, 123530.

19 D. Yan, M.-M. Ren, F.-F. Mao, Y. Ma, R.-L. Tang, B. Zhang, Y. Ma, X.-D. Zhang, S.-F. Li, *Inorg. Chem.* 2023, **62**, 1323–1327.

20 Y. Huang, X. Meng, P. Gong, L. Yang, Z. Lin, X. Chen, J. Qin, *J. Mater. Chem. C* 2014, **2**, 4057–4062.

21 H. Song, N. Wang, Y. Li, W. Liu, Z. Lin, J. Yao, G. Zhang, *Solid State Sciences* 2019, **97**, 105982.

22 Q.-Q. Chen, C.-L. Hu, J. Chen, Y.-L. Li, B.-X. Li, J.-G. Mao, *Angew. Chem. Int. Ed.* 2021, **60**, 17426–17429.

23 Y. Xu, Y. Zhou, C. Lin, B. Li, X. Hao, N. Ye, M. Luo, *Cryst. Growth Des.* 2021, **21**, 7098–7103.

24 L. Zhu, M. Gai, W. Jin, Y. Yang, Z. Yang, S. Pan, *Inorg. Chem. Front.* 2021, **8**, 3127-3133.

25 M. Gai, T. Tong, Y. Wang, Z. Yang, S. Pan, *Chem. Mater.* 2020, **32**, 5723-5728.